Journal of Alloys and Compounds 578 (2013) 170–175

Contents lists available at SciVerse ScienceDirect

Journal of Alloys and Compounds

journal homepage: www.elsevier.com/locate/jalcom

Irradiation effect on the structure change for $Sr_2Fe_{1.5}Mo_{0.5}O_{6-\delta}$ perovskite ceramic

Siwei Wang [a,b], Ming Tang [b,*], Lingling Zhang [a], Guoliang Xiao [a], Kyle S. Brinkman [c], Fanglin Chen [a,*]

[a] Department of Mechanical Engineering, University of South Carolina, Columbia, SC 29208, USA
[b] Materials Science and Technology Division, Los Alamos National Laboratory, Los Alamos, NM 87545, USA
[c] Science and Technology Directorate, Savannah River National Laboratory, Aiken, SC 29808, USA

ARTICLE INFO

Article history:
Received 31 March 2013
Received in revised form 22 April 2013
Accepted 23 April 2013
Available online 15 May 2013

Keywords:
Irradiation
Perovskite
Decomposition
Reduction
Nano-crystals

ABSTRACT

The incorporation of radioactive elements derived from fission products (FPs) into a stabilized crystalline structure is an active area of research in the nuclear fuel cycle. The compound $Sr_2Fe_{1.5}Mo_{0.5}O_{6-\delta}$ (SFM) incorporates several FPs (Sr and Mo) into the crystalline network simultaneously while maintaining a stabilized perovskite structure. This polycrystalline SFM sample was irradiated with 200 keV He ions to a fluence of 5×10^{16} ions cm^{-2} (corresponding to a peak dose at 1.2 dpa) at room temperature to study radiation damage effects. Irradiated SFM sample decomposed into a layered $Sr_4FeMoO_{8-\delta}$ based phase and a Fe metallic phase, resulting in nano-crystalized grains with particle sizes around 7 nm. It was rationalized that He ion irradiation created a reduced atmosphere on the surface of SFM sample by preferentially sputtering oxygen atoms, consequently decomposing SFM and reducing Fe ions into metallic Fe phases. These results suggest that the stability of crystalline structures in reducing atmospheres may be an additional factor for consideration in the search for FP hosts in crystalline materials.

1. Introduction

It is currently envisioned that high-level radioactive waste (HLW) arising from the reprocessing of spent nuclear fuel (SNF) will be immobilized in a vitreous waste form such as alkali borosilicate glasses [1,2]. However, there have long been concerns regarding devitrification of HLW glass because certain fission product (FP) species prefer to reside in crystalline phases, rather than in the glass matrix. Thus, the incorporation of radioactive elements in FPs into a stabilized crystalline network, where the elements are constrained in the structure resulting in enhanced leaching and radioactive stability, is an active area of research in the nuclear fuel cycle [3–5]. The most extensive investigations have focused on the Synroc waste forms (including rutile structured titanium oxides), fluorite structured oxides, pyrochlore structured oxides, and the complex M_7O_{12} delta crystal structured oxide compounds [6–11]. Recently the perovskite structured compounds have attracted increased attention due to their superior performance under irradiation conditions simulating decay in realistic storage environments [12,13]. The perovskites and related structured crystalline materials have been widely studied in many areas including dielectrics, ferromagnetics, superconductors and fuel cells. One unique property of the perovskite is that it remains a stable structure within the tolerance factor t ranging from 0.78 to 1.05, where t is a description of degree of distortion and is defined as:

$$t = \frac{r_A + r_O}{\sqrt{2}(r_B + r_O)} \quad (1)$$

where r_A, r_B, and r_O are the ionic radii of A, B and O, respectively for the perovskite with a formula of ABO_3. Due to such a large tolerance range, it is possible to accommodate FPs such as ^{90}Sr, Mo, and any of the lanthanides (Ln) (or alternatively, ^{99}Tc, and ^{137}Cs), into the crystalline network simultaneously while maintaining the stabilized perovskite structure.

This study focuses on the irradiation effects of the perovskite phase $Sr_2Fe_{1.5}Mo_{0.5}O_{6-\delta}$ (denoted as SFM afterwards) oxide material which simultaneously incorporates Sr and Mo FPs into the crystalline structure. Mo doped $SrFeO_3$ was previously investigated as magnetoresistive materials and solid oxide fuel cell electrode materials [14–16]. $Sr_2Fe_{1.5}Mo_{0.5}O_{6-\delta}$ is traditionally written as a double perovskite structure, where 1/4 of B sites are occupied by Mo. The crystal structure of SFM is *Fm-3m*, with lattice parameter $a = 7.8717$ Å (PDF#97-009-6223) [17]. While it has been later revealed that unlike other ordered double perovskites, the Mo and Fe atoms randomly occupy rather than orderly distribute in the B and B' sites, thus it is actually a simple perovskite structured oxide with proposed *Pm-3m* structure [18]. Recent detailed neutron diffraction study on SFM further suggests a *Pnma* structure and that the structure of this material is very sensitive to the concentration

* Corresponding authors. Tel.: +1 505 665 1472 (M. Tang), tel.: +1 803 777 4875 (F. Chen).
E-mail addresses: mtang@lanl.gov (M. Tang), chenfa@cec.sc.edu (F. Chen).

0925-8388/$ - see front matter © 2013 Elsevier B.V. All rights reserved.
http://dx.doi.org/10.1016/j.jallcom.2013.04.166

of oxygen vacancies [19]. In this study, we are focusing on the irradiation effect on the perovskite SFM material. The radiation induced structural changes, including the decomposition of the material and appearance of secondary phases, as well as lattice changes of SFM has been evaluated.

2. Experimental

SFM powder was prepared by a modified Pechini method as reported previously [15,20,21]. The metal nitrates were titrated and dissolved stoichiometrically in glycine and citric acid solutions, combusted to ashes, followed by firing the as-prepared ash powder at 1000 °C for 5 h. The powder was then pressed into pellets and sintered at 1300 °C for 4 h. The as sintered pellets were cut into pieces and polished for further investigation. In preparation for ion irradiation, all samples were finally polished with a 40 nm colloidal silica slurry (Syton HT50, DuPont Air Products NanoMaterials L.L.C, Tempe, AZ), in order to remove the surface damage created by the previous mechanical polishing steps. Ion irradiation experiments were performed at room temperature (~25 °C) at the Ion Beam Materials Laboratory, Los Alamos National Laboratory, using a 200 kV Danfysik high current research ion implanter. 200 keV He^+ ions were implanted at normal incident using a flux of 2×10^{12} ions cm^{-2} s^{-1} to a fluence of 5×10^{16} ions cm^{-2}. The overall surface structural information for the irradiated sample was collected by a grazing angle incident X-ray (GIXRD) diffractometer (Bruker AXS D8 Advanced X-ray diffractometer with a Cu Kα radiation and a graphite monochromator)), and θ–2θ geometry. The step size of the scan angle was 0.02° with the dwell time 4 s per step. The scan range was 20–80° under X-ray incident angles from 0.25° to 3°. Irradiated sample was also prepared in cross-sectional geometries for transmission electron microscopy (TEM) examination. The microstructural evolution of the irradiated sample was characterized by a TEM (Fei Tecnai F30) with a point-to-point resolution of 0.21 nm operating at 300 kV. Raman spectroscopy (HORBIA, Jobin Yvon) was employed to determine the local structural bonding environmental changes due to the irradiation.

3. Results and discussion

3.1. SRIM simulation

The stopping and range of ions in matter (SRIM) Monte Carlo program [22] was used to simulate the displacement damage profile in SFM caused by He ion irradiation as shown in Fig. 1. A threshold displacement energy of 40 eV (an arbitrary assumption) was used for all target elements. This simulation predicts that the peak displacement damage dose is ~1.2 displacements per atom (dpa) at a sample depth of 630 nm, while the He concentration reaches a maximum of 2.4% He atom when it goes into the depth of 690 nm.

3.2. Structural evolution

The SRIM simulation results which indicate thin layer irradiation on the SFM surface prompt us to employ GIXRD with small incident angles to characterize the structural evolution on the surface. The critical angle α_c within which total external reflection occurs for the X-ray can be calculated by the critical angle calculation [23,24]. α_c is given by following equation:

$$\alpha_c = 1.6 \times 10^{-3} \rho^{1/2} \lambda \quad (2)$$

where ρ is the density of material in g cm^{-3} (5.487 g cm^{-3} for SFM), and λ is the wavelength of X-ray in Å (1.5406 Å) [25]. In our case the α_c is calculated to be 0.33°. The penetration depth is then calculated by the following two equations:

$$L = \lambda / 2\pi(\alpha_c^2 - \alpha^2)^{1/2} \ (\text{for } \alpha < \alpha_c) \quad (3)$$

$$L = 2\alpha/\mu \ (\text{for } \alpha > \alpha_c) \quad (4)$$

where μ is the linear attenuation coefficient (7.5×10^2 cm^{-1} for SFM based on our calculation [26]). The calculated values of penetration depth are shown in Fig. 2. GIXRD was conducted with incident angles of 0.25°, 0.5°, 0.75°, 1° and 3° respectively, to cover the critical angle and the penetration depth range.

XRD results reveal that the desired single phase perovskite SFM is obtained using the above fabrication method as shown in Fig. 3a, denoted as pristine sample. The structure information has been reported in our previous publication, showing a cubic perovskite *Pm-3m* structure, with lattice parameter $a = 3.9287$ Å, which is equivalent to that of SFM with *Fm-3m* structure if transformed into a cubic double perovskite structure [18]. Irradiation induced significant structural evolution in SFM, as can be observed from the GIXRD measurements. As shown in Fig. 3a, from the patterns of the irradiated samples, the additional peaks can be identified as Fe (PDF #97-005-3451) and layered $Sr_4FeMoO_{8-\delta}$ (PDF # 97-015-2243) based composites. It is interesting that SFM was decomposed and the Fe ions were reduced into metallic Fe phase. It was reported that for metal oxides (binary oxides such a FeO, Fe_2O_3, CoO, TiO_2 and Nb_2O_5), the reduction in oxidation state caused by ion bombardment could be accounted for the preferential removal of oxygen and ion-induced oxide reduction [27–29]. Similarly, in our case, such kind of ion-induced reduction in oxidation state in perovskite structured SFM may be also due to the preferential sputtering of oxygen atoms from the oxide matrix. The mechanism can be understood through a collisional approach to explain the average composition of metal-to-oxygen concentration ratio [28], or a thermal approach to explain specific stoichiometries [29].

It is worth noting that the presence of metallic Fe may also be understood as the reduction of ionic Fe ions. The preferential sputtering of oxygen atoms from oxide matrix bears an analogy to the reduction of ionic Fe ions into metallic Fe. This is plausible since in

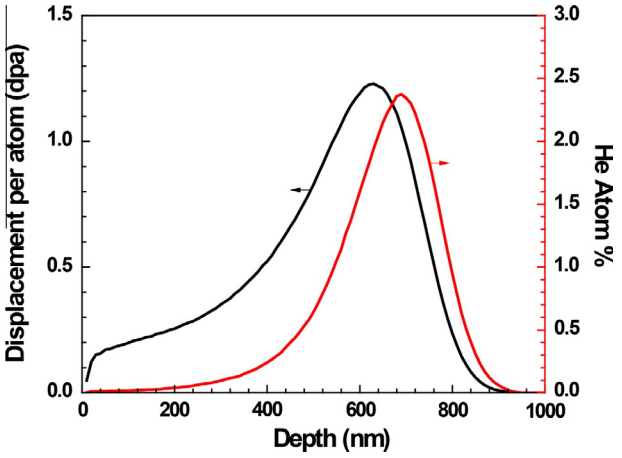

Fig. 1. SRIM simulation results for 200 keV He ion irradiated into SFM at 5×10^{16} ions cm^{-2}.

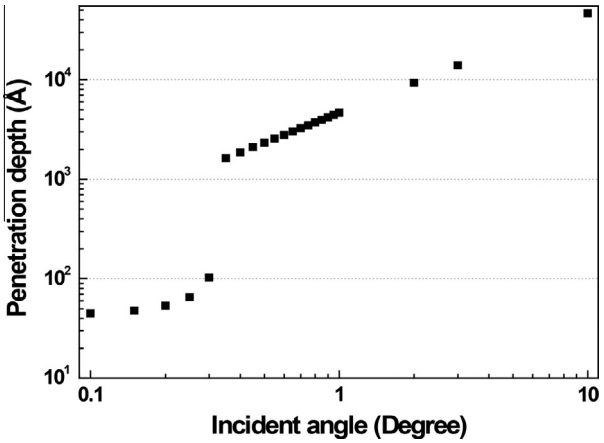

Fig. 2. Calculated GIXRD scattering depth in SFM.

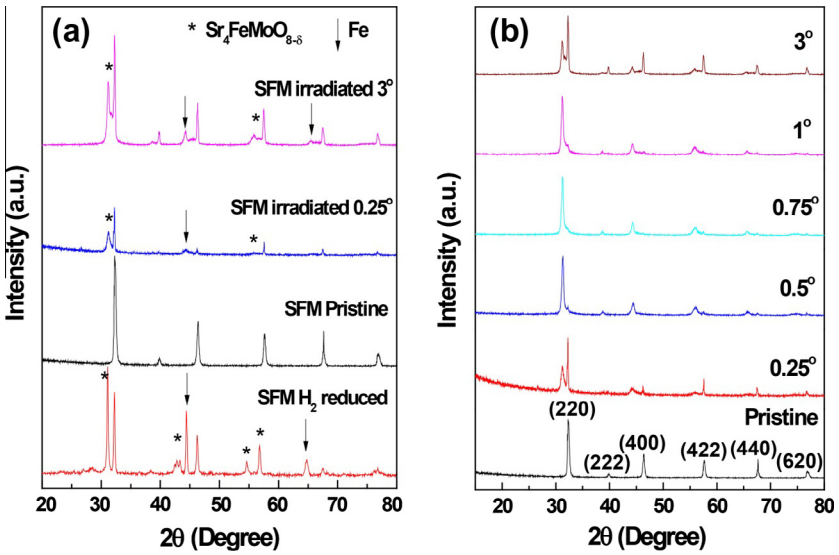

Fig. 3. (a) Comparison of XRD patterns for pristine, He ion irradiated, and H_2 reduced SFM samples and (b) GIXRD patterns for He ion irradiated sample with different incident angles.

the irradiation experiment, the low oxygen partial pressure in the environment (10^{-9}–10^{-10} atm for the vacuum system) as well as the high energy He ion beam irradiation preferentially knocked the oxygen atoms off into interstitials and locally displaced oxygen atoms, providing a very reducing environment in the "local" conditions of the structure. Such "locally" reducing environment leads to oxygen vacancies in the lattice and the formation of metallic Fe phase and a Fe deficient (compared with SFM) layered structured $Sr_4FeMoO_{8-\delta}$ based phase. The reduction of Fe ion into Fe metal under He ion irradiation as reported in perovskite ceramic is the first known occurrence of this phenomenon.

To confirm that He irradiation reduced the Fe ions into Fe metal for the SFM sample, the pristine SFM sample powder was treated in reduced H_2 atmosphere at 900 °C for 10 h as comparison. It can be seen from Fig. 3a that the XRD pattern of irradiated SFM is very similar to that of the reduced SFM. After H_2 reduction at high temperatures, SFM decomposed via the following equation:

$$2Sr_2Fe_{1.5}Mo_{0.5}O_{6-\delta} = 2Fe + Sr_4FeMoO_{8-\delta} \quad (5)$$

The similar XRD spectra between the H_2 and He irradiation experiments validate the hypothesis that the He irradiation may have resulted in a locally extremely reducing condition for the irradiated SFM sample. It should be noted that similar to $Sr_2Fe_{1.5}Mo_{0.5}O_{6-\delta}$ which deviated from $Sr_2FeMoO_{6-\delta}$ based composition, the decomposed $Sr_4FeMoO_{8-\delta}$ only represents the base secondary phase. In other words, the Fe/Mo ratio in the secondary phase is not determined to be 1:1 and can be varied.

As shown in Fig. 3b, for the GIXRD patterns of the irradiated sample, at incident angle of 0.25°, the additional peaks show up along with the peaks of the SFM phase, implying that the content of the secondary phases are comparable with the SFM phase at this specific X-ray penetration depth (very top surface based on calculation in Fig. 2). For incident angles from 0.5° to 1°, the secondary phases predominant over the SFM phase, implying that most of SFM has been decomposed into secondary phases at these corresponding penetration depths. When the incident angle further increases to 3°, the relative intensity of the secondary phases decreases, indicating that with further increase in penetration depth (deeper than 1000 nm in our calculation as shown in Fig. 2), the X-ray penetrated the irradiation layer and reached the unirradiated SFM substrate whose information was also collected. This is in agreement with the SRIM calculation that the irradiation occurs at below 1000 nm, where He ions preferentially knock oxygen off, and the reduction of Fe ion into Fe metal occurs.

3.3. TEM microstructural characterization

The configuration of the TEM sample is shown in Fig. 4a. From Fig. 4a the global information about the components of the TEM sample and the different morphologies for the unirradiated and irradiated layers can be clearly identified. The unirradiated substrate shows light gray background with scratches on the surface, while the ion irradiated damage layer shows dark gray color with coarsened morphology. The thickness of the ion irradiated damage layer is around 820 nm, consistent with the SRIM simulation result. SAED experiments were performed for the TEM sample with a probe size of 100 nm to examine the localized variation of lattice distortions along the irradiation path. Fig. 4b and c shows the corresponding SAED patterns along $[\bar{1}\,1\,3]$ zone axis for the unirradiated SFM substrate and the irradiated damage layer, respectively. For the unirradiated substrate layer, the calculated d-spacing for the (220) peak is 0.2759 nm. While for the ion irradiated damage layer, from the SAED pattern shown in Fig. 4c, the d-spacing for the (220) peak is around 0.2770 nm. The lattice parameter of the ion irradiated damage layer was expanded by 0.40%, which is unlikely to be caused by the swelling of the base SFM material as the lattice expansion calculated from the base SFM peak is much smaller (less than 0.20% in lattice expansion for (220) peak). In addition the relative intensity of SFM is quite weak as seen from the XRD patterns in Fig. 3b. Such SAED pattern may be caused by the appearance of the secondary $Sr_4FeMoO_{8-\delta}$ based phase with an ordered structure. For example, for ordered $Sr_4FeMoO_{8-\delta}$, the (110) peak is 0.2771 nm, very close to the value obtained from the observed SAED pattern. Further study to determine the stoichiometric composition of $Sr_4FeMoO_{8-\delta}$ and the Fe content will be conducted.

Fig. 5a shows SAED pattern of the pristine SFM sample along $[\bar{1}\,1\,1]$ zone axis. The d-spacing for the (220) peak is calculated to be 0.2762 nm, consistent with that of the irradiated SFM substrate along $[\bar{1}\,1\,3]$ zone axis. The corresponding high resolution image of the unirradiated substrate along $[\bar{1}\,1\,1]$ zone axis is shown in Fig. 5b, with the inset the expanded view of selected area. It can be seen that the pristine SFM sample is crystalized with clear fringes and structures. Fig. 6a shows the SAED pattern of ion irradiated damage layer along $[\bar{1}\,1\,3]$ zone and Fig. 6b is the high

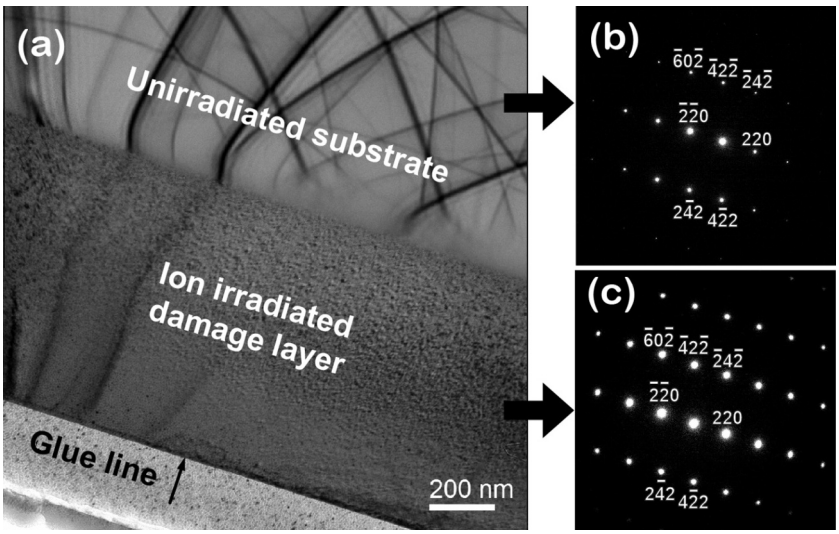

Fig. 4. (a) TEM image of the irradiated SFM sample; (b) SAED pattern of unirradiated SFM substrate along the [$\bar{1}$ 1 3] zone axis, and (c) SAED pattern of ion irradiated damage layer along the [$\bar{1}$ 1 3] zone axis of the sample.

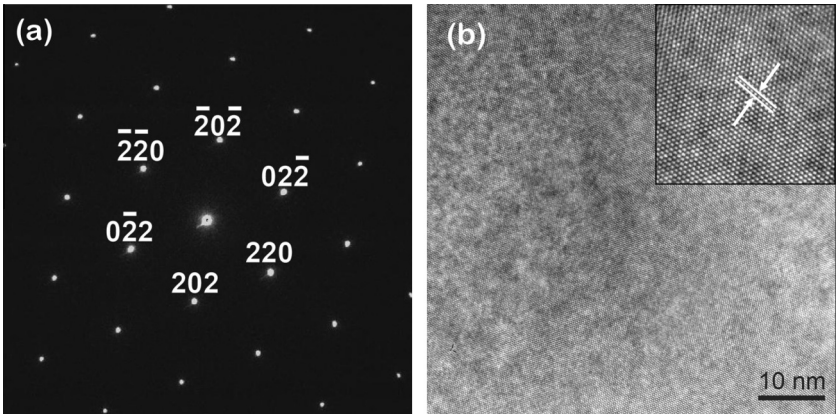

Fig. 5. (a) SAED pattern of pristine SFM sample along the [$\bar{1}$ 1 1] zone axis, (b) HRTEM image corresponding to the [$\bar{1}$ 1 1] zone axis of the pristine SFM sample, inset is the expanded view of selected area.

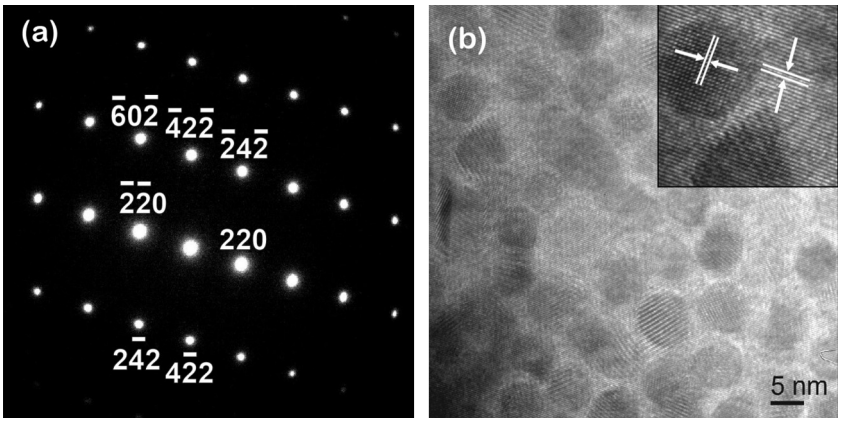

Fig. 6. (a) SAED pattern of the irradiated SFM sample along the [$\bar{1}$ 1 3] zone axis, and (b) HRTEM image corresponding to the [$\bar{1}$ 1 3] zone axis of the irradiated SFM sample, inset is the expanded view of selected area.

resolution TEM image of ion irradiated damage layer and inset is the expanded view of selected area. No irradiation-induced amorphization is observed for the irradiated sample. However, different from the morphology shown in Fig. 5b, it can be clearly seen from Fig. 6b that sphere like nano-crystals are distributed uniformly in the ion irradiated damage layer with average grain size around 7 nm. It is difficult to determine from the TEM images what the exact structural information is for the nano-crystals, but it is

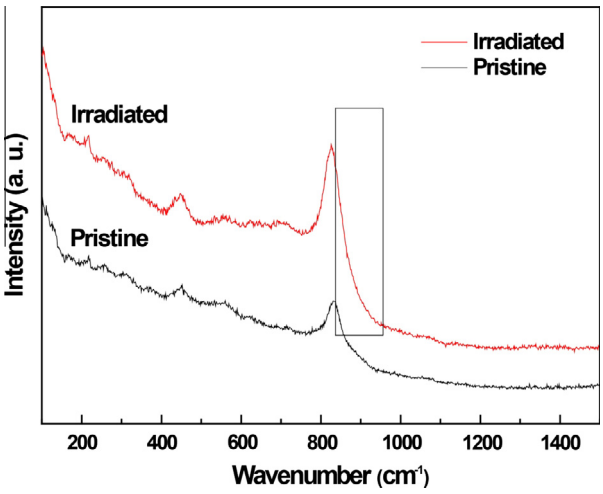

Fig. 7. Raman spectra of the pristine and irradiated SFM sample surfaces.

determined that the nano-crystals are well crystalized, and the crystal structures of these nano-crystals are clearly different from the background lattices (see Fig. 6b inset). The background lattice orientation and lattice parameter are consistent with the information obtained from XRD and SAED results that it is $[\bar{1}\,1\,3]$ zone axis oriented.

3.4. Raman spectroscopy

Fig. 7 shows the Raman spectroscopies of the pristine and irradiated SFM samples excited at 632.8 nm with a He–Ne laser. Raman spectra excited at 441.6 nm (He–Cd laser, which penetrates shorter distances in the samples) showed no difference (not shown here), indicating that surface information was collected in both spectra. It is known that the phonon modes for $SrFeO_{3-x}$ based materials strongly depend on the oxygenated level, and are related to the oxygen vacancy of the materials (which is difficult to control [19]). The peaks for the Raman spectra are thus difficult to identify [30]. Nevertheless, for the SFM spectrum, the strongest peak at around 830 cm^{-1} is characteristic of $Sr_2Fe_{1+x}Mo_{1-x}O_{6-\delta}$ [31], which is related to the breathing vibration of oxygen in $(Fe/Mo)O_6$ octahedral and sensitive to B-site substitution as that can be identified in Fig. 7 [32]. It can be seen that the two spectra show similar peaks and peak intensities, while the peak positions for the irradiated sample show a clear red shift of around 7 cm^{-1} (shifting to lower wavenumber). The red[1] shift for Raman spectroscopy is essentially caused by the lowering energy required for the vibration, which may be due to the optical phonon confinement, defect or impurity in the material, laser irradiation heating, the tensile strain effect, and the residual stress [33]. It is apparent that the irradiation introduced new phases on the surface and the $Sr_4FeMoO_{8-\delta}$ will affect the peak position of the $(Fe/Mo)O_6$ mode. Surface atoms of nano-particles are bound by weaker forces because of missing neighbors, leading to lower energy and lower characteristic wavenumbers [34]. It is also possible that the surface strain affected the surface structure, resulting in shifts and broadening of the Raman peaks [34,35]. It is noted that the characteristic peak for $SrMoO_4$ at 882.3 cm^{-1} is not seen [30,31]. The characteristic peaks for Fe_3O_4 and Fe_2O_3 are not observed either [36]. Nor could we identify Fe peaks due to the strong $(Fe/Mo)O_6$ peak at around 883 cm^{-1} or the intensity not high enough to be detected on the irradiated sample surface. The Raman spectroscopy thus suggests that the secondary $Sr_4FeMoO_{8-\delta}$ based phase affected the peak position of the $(Fe/Mo)O_6$ mode, leading to the red shift of the Raman scattering peaks.

[1] For interpretation of color in Fig. 7, the reader is referred to the web version of this article.

3.5. Discussion

We report for the first time the decomposition and reduction of SFM ceramic into nano-crystals under He ion irradiation. He ion irradiation preferentially sputtered oxygen atoms off the structure of SFM, reducing Fe ions into Fe metals, and the ramification of which was the formation of $Sr_4FeMoO_{8-\delta}$ based phase. Such decomposition and reduction led to the precipitation of nano-crystals with average sizes around 7 nm. The mechanism and results of the reduction process are analogous to the reduction of SFM in reducing atmospheres, where in both situations the oxygen atoms are taken off the structure. The equivalent "local" oxygen partial pressure the He ion irradiation provides should depend on the energy and fluence of the irradiation, while the decomposition of the material should depend on the oxygen partial pressure the He irradiation provides, the intensity of the ion beam bombardment, and the stability of the material itself. It further suggests that the He irradiation may provide a "locally" very reducing environment for the materials, and thus the stability in reducing atmospheres may be one critical criterion for searching potential nuclear waste form materials. In other words, if a material is chemically not stable in reducing atmospheres, it will probably suffer decomposition under high energy He ion irradiation.

4. Conclusions

The irradiation effect on $Sr_2Fe_{1.5}Mo_{0.5}O_{6-\delta}$ perovskite structured oxide ceramic has been evaluated. No irradiation-induced amorphization was observed in SFM under 200 keV He irradiation at room temperature; while He irradiation preferentially sputtered oxygen atoms off the structure, providing a locally very reducing environment for the material, decomposing SFM into metallic Fe and layered structured $Sr_4FeMoO_{8-\delta}$ based phase, leaving a nano-crystalized structured morphology. These results suggest that a potential criterion applied for radiation tolerance of nuclear wastes or advanced nuclear fuel forms, is the structural stability of the materials in locally reducing atmospheres arising from fission product decay in the crystalline matrix.

Acknowledgements

The financial supports from the US Department of Energy, Office of Nuclear Energy's Fuel Cycle Research & Development (FCR&D) programs and Nuclear Energy University Programs (NEUP) are gratefully acknowledged. SW would also like to thank the Seaborg Institute Summer Fellowship program sponsored by the Seaborg Institute for Transactinium Science, Los Alamos National Laboratory.

References

[1] Committee on Waste Forms Technology and Performance; National Research Council, Waste Forms Technology and Performance: Final Report, The National Academics Press, Washington, DC, 2011.
[2] D. Gombert, Global nuclear energy partnership-materials disposition and waste form status, in: Report, GNEP-WAST-AI-TR-2007-00013, 2007.
[3] M.L. Carter, A.L. Gillen, K. Olufson, E.R. Vance, J. Am. Ceram. Soc. 92 (2009) 1112–1117.
[4] S.V. Stefanovsky, A.G. Ptashkin, O.A. Knyazev, S.A. Dmitriev, S.V. Yudintsev, B.S. Nikonov, J. Alloys Comp. 444–445 (2007) 438–442.
[5] K. Brinkman, K. Fox, J. Marra, J. Reppert, J. Crum, M. Tang, J. Alloys Comp. 551 (2013) 136–142.
[6] A.E. Ringwood, S.E. Kesson, N.G. Ware, W. Hibberson, A. Major, Nature 278 (1979) 219–223.
[7] K.E. Sickafus, R.W. Grimes, J.A. Valdez, A. Cleave, M. Tang, M. Ishimaru, S.M. Corish, C.R. Stanek, B.P. Uberuaga, Nat. Mater. 6 (2007) 217–223.

[8] M. Lang, F. Zhang, J. Zhang, J. Wang, J. Lian, W.J. Weber, B. Schuster, C. Trautmann, R. Neumann, R.C. Ewing, Nucl. Instrum. Methods Phys. Res. Sect. B 268 (2010) 2951–2959.
[9] R.C. Ewing, W.J. Weber, J. Lian, J. Appl. Phys. 95 (2004) 5949–5971.
[10] K.E. Sickafus, H. Matzke, T. Hartmann, K. Yasuda, J.A. Valdez, P. Chodak Iii, M. Nastasi, R.A. Verrall, J. Nucl. Mater. 274 (1999) 66–77.
[11] M. Ishimaru, Y. Hirotsu, M. Tang, J.A. Valdez, K.E. Sickafus, J. Appl. Phys. 102 (2007) 063532.
[12] B. Tsuchiya, S. Nagata, K. Toh, T. Shikama, Nucl. Instrum. Methods Phys. Res., Sect. B 242 (2006) 588–590.
[13] Y. Zhang, J. Lian, Z. Zhu, W.D. Bennett, L.V. Saraf, J.L. Rausch, C.A. Hendricks, R.C. Ewing, W.J. Weber, J. Nucl. Mater. 389 (2009) 303–310.
[14] T. Yamamoto, J. Liimatainen, J. Linden, M. Karppinen, H. Yamauchi, J. Mater. Chem. 10 (2000) 2342–2345.
[15] G. Xiao, Q. Liu, S. Wang, V.G. Komvokis, M.D. Amiridis, A. Heyden, S. Ma, F. Chen, J. Power Sources 202 (2012) 63–69.
[16] Q. Liu, X. Dong, G. Xiao, F. Zhao, F. Chen, Adv. Mater. 22 (2010) 5478–5482.
[17] G. Liu, G. Rao, X. Feng, H. Yang, Z. Ouyang, W. Liu, J. Liang, J. Alloys Comp. 353 (2003) 42–47.
[18] Q. Liu, D.E. Bugaris, G. Xiao, M. Chmara, S. Ma, H.-C. zur Loye, M.D. Amiridis, F. Chen, J. Power Sources 196 (2011) 9148–9153.
[19] A.B. Muñoz-García, D.E. Bugaris, M. Pavone, J.P. Hodges, A. Huq, F. Chen, H.-C. zur Loye, E.A. Carter, J. Am. Chem. Soc. 134 (2012) 6826–6833.
[20] S. Wang, F. Zhao, L. Zhang, F. Chen, Solid State Ionics 213 (2012) 29–35.
[21] S. Wang, F. Zhao, L. Zhang, K. Brinkman, F. Chen, J. Alloys Comp. 506 (2010) 263–267.
[22] J.F. Ziefler, J.P. Biersack, U. Littmark, The stopping and Range of Ions in Solids, Pergamon, New York, 1985.
[23] A. Guinier, X-ray Diffraction in Crystals, Imperfect Crystals and Amorphous Bodies, Dover Publications, Inc., Mineola, New York, 1994.
[24] D. Rafaja, V. Valvoda, A.J. Perry, J.R. Treglio, Surf. Coat. Technol. 92 (1997) 135–141.
[25] M. Tang, Ph.D thesis: radiation damage effects in rare earth sesquioxides under ion irradiation, New Mexico Institute of Mining and Technology, Socorro, New Mexico, 2006.
[26] B.D. Cullity, Elements of X-ray Diffraction, Addison-Wesley Publishing Company, Inc., Reading, Massachusetts, 1956.
[27] T. Choudhury, S.O. Saied, J.L. Sullivan, A.M. Abbot, J. Phys. D: Appl. Phys. 22 (1989) 1185–1195.
[28] J.B. Malherbe, S. Hofmann, J.M. Sanz, Appl. Surf. Sci. 27 (1986) 355–365.
[29] R. Kelly, Surf. Sci. 100 (1980) 85–107.
[30] L.H. Son, N.X. Phuc, P.V. Phuc, N.M. Hong, L.V. Hong, J. Raman Spectrosc. 32 (2001) 817–820.
[31] C. Yuan, Y. Zhu, P.P. Ong, C.K. Ong, T. Yu, Z. Shen, Physica B 334 (2003) 408–412.
[32] S. Ye, C. Wang, X. Jing, J. Electrochem. Soc. 155 (2008) J148–J151.
[33] R. Zhang, P. Yin, N. Wang, L. Guo, Solid State Sci. 11 (2009) 865–869.
[34] C. Xu, P. Zhang, L. Yan, J. Raman Spectrosc. 32 (2001) 862–865.
[35] J.F. Mammone, S.K. Sharma, M. Nicol, Solid State Commun. 34 (1980) 799–802.
[36] Raman spectra database of minerals and inorganic materials. <http://riodb.ibase.aist.go.jp/db092/E_index_list.html>.